Propagation of desynchronous disturbances in synchronized chaotic one-way coupled map lattices

Huaping Lü[1,2] and Gang Hu[3,1,4]
[1]*Department of Physics, Beijing Normal University, Beijing 100875, China*
[2]*Department of Physics, Xuzhou Normal University, Xuzhou 221009, China*
[3]*China Center for Advanced Science and Technology (CCAST) (World Laboratory), P.O. Box 8730, Beijing 100080, China*
[4]*The Key Laboratory of Beam Technology and Material Modification of Ministry of Education, Beijing Normal University, Beijing 100875, China*

(Received 18 October 2003; revised manuscript received 25 November 2003; published 31 March 2004)

Propagations of desynchronous perturbations in synchronization processes of spatiotemporal chaos are investigated by considering chaotic one-way coupled map lattices. Under large coupling approximation the desynchronous area in time space is analytically calculated, based on the concepts of comoving Lyapunov exponent and absolute largest Lyapunov exponent. The ideas used in this paper are expected to be applicable to synchronizations of spatiotemporally chaotic systems of coupled maps and coupled oscillators with convective instability.

DOI: 10.1103/PhysRevE.69.036212 PACS number(s): 05.45.Ra

In the recent decade, investigations of dynamic behavior and control and synchronization of spatiotemporal chaos have attracted much attention due to both theoretical interest and hopeful anticipation of wide applications; see Refs. [1–12] for recent review. For practical spatiotemporal chaos control and synchronization, we hope to use a small number of control signals to control and synchronize systems with large space, or say, with many positive Lyapunov exponents (LEs). It is particularly desirable if we can reach so high control efficiency that a single injected time sequence can successfully control and synchronize spatiotemporal chaos with arbitrarily large space length and arbitrarily large dimensionality. In doing so, an effective and undamped propagation of control (synchronization) signal in space becomes the key point. It is now well understood that spatiotemporal systems with large gradient couplings (or say, with strongly asymmetrical couplings in coupled map lattices) can effectively propagate control signals and can be used as ideal systems for spatiotemporal chaos control and synchronization [13–16]. One-way coupled chaotic map lattices belong to typical systems of this kind [14,17–19].

It is also known that some spatial systems with strong gradient coupling may show convective instability under the absolute stability condition. This convective instability is the key reason for the effective propagation of control signals [20–22]. On the other hand, with convective instability, any out-control (desynchronization) disturbances may be considerably amplified, and widely spread and easily propagated along the direction of the gradient coupling. This amplification and propagation of disturbances may cause serious problems for the applicability of various control methods. For instance, when we perform secure communication by synchronizing spatiotemporal chaos [23,24], the disturbance propagation is closely related to the so-called avalanche effect of data errors (i.e., a single data error in the input signal may cause errors of huge output data). Thus, a comprehensive theoretical understanding on the disturbance propagation problem in controlled spatiotemporal systems is of crucial importance for practical applications of chaos control and synchronization. To our knowledge, this problem has not yet been thoroughly studied, and it is the central task of the present paper.

In this paper we focus on propagations of desynchronous perturbations in spatiotemporal chaos synchronization processes. We take chaotic one-way coupled map lattices as our model, and the ideas are expected to be applicable to wide range of spatiotemporal systems with convective instability and absolute stability. We start with the following driving system, a one-way coupled ring map lattice [see Fig. 1(a) for the schematic diagram],

$$x_{n+1}(i)=(1-\varepsilon)f[x_n(i)]+\varepsilon f[x_n(i-1)], \tag{1}$$

$$i=1,2,\ldots,L, \quad x_n(0)=x_n(L). \tag{2}$$

Without losing any generality we use the fully developed chaotic logistic function for the map

$$f(x)=4x(1-x). \tag{3}$$

With the ring structure of Fig. 1(a), the system is spatiotemporal chaos with very high dimensionality for $L\gg 1$ and for most of choices of coupling ε (except some periodic windows). From Eq. (2) we output a driving signal $x_n(0)=x_n(L)$, and use this signal to drive a one-way coupled open map lattice (OCOML) [Fig. 1(b)]

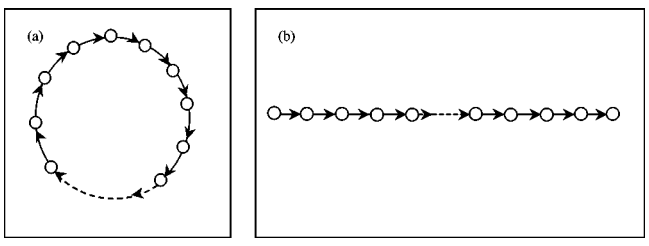

FIG. 1. The schematic diagram of the model. (a) One-way coupled ring map lattice (OCRML); (b) one-way coupled open map lattice (OCOML).

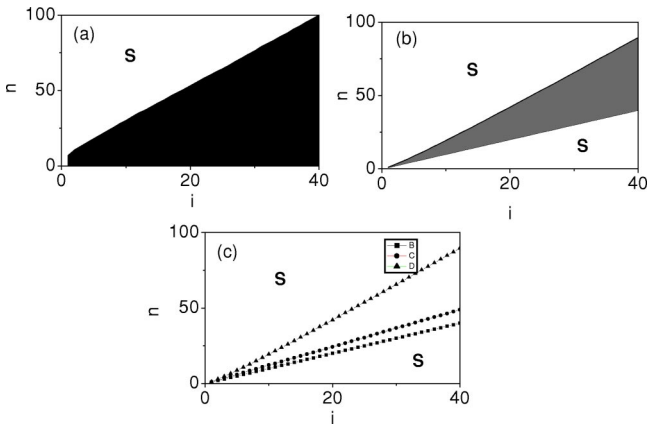

FIG. 2. $\varepsilon=0.8$. Distributions of synchronization (denoted by S) and desynchronization (black area) regions. Synchronization is assumed if $\Delta_n(i)=|y_n(i)-x_n(i)|\leqslant r=10^{-10}$. (a) With a single driving sequence $y_n(0)=x_0(0)$ only, system (4) fast synchronizes with system (1). (b) Supposing systems (4) and (1) are synchronized at $n<0$, and then setting small data error $\delta_0=10^{-10}$ on the driving of the first site at $n=0$ as Eq. (8), synchronization between systems (4) and (1) is broken temporarily (black area), and recovered again after a certain time (the upper S area). (c) Lines *B* and *D* are the lower and upper boundaries of the desynchronous area in (b), respectively; line *C* is the time position when the desynchronous values of various sites, $\delta_n(i)$, reach their maximum over the iteration numbers (each plot is obtained by averaging data of 1000 runs).

$$y_{n+1}(i)=(1-\varepsilon)f[y_n(i)]+\varepsilon f[y_n(i-1)],$$

$$i=1,2,\ldots,L, \quad y_n(0)=x_n(0). \tag{4}$$

For sufficiently large ε (e.g., $\varepsilon\geqslant 0.75$), the trajectory of system (4) can be fully synchronized to the trajectory of system (1) after certain transient period. In Fig. 2(a) we plot difference $\Delta_n(i)=|y_n(i)-x_n(i)|$ from arbitrary initial conditions of $x_0(i)$ and $y_0(i)$ for $\varepsilon=0.8$. In Fig. 2, synchronization is assumed whenever $\Delta_n(i)\leqslant r=10^{-10}$, and desynchronization is identified otherwise. It is remarkable that with a single driving sequence $y_n(0)=x_n(0)$ only, all the sites of system (4) can be exactly synchronized to the corresponding sites of system (1) eventually no matter how large the system size ($L\gg 1$) is and how turbulent system (1) is [note, with $L\gg 1$, system (1) is spatiotemporal chaos with a huge number of positive LEs].

Nevertheless, the above desirable advantage also causes an undesirable problem, i.e., the synchronization of Eq. (4) becomes sensitive to small perturbation of the driving, and can be largely (though temporarily) disturbed by any data error in the input. We set a small data error $|y_0(0)-x_0(0)|=\delta_0$ with $\delta_0=10^{-10}$ at time $n=0$ under the condition of existing full synchronization between Eqs. (4) and (1). This small error at a single site and a single time can develop a large desynchronization wave as shown in Fig. 2(b). The desynchronous wave has the following characteristics. First, the wave moves from small i to large i (from upstream to downstream), and the desynchronous error is amplified as the wave moves. This indicates a convective (moving) instability. Second, if we focus on a given site [say $y_n(i)$ with fixed i], the desynchronous element $|y_n(i)-x_n(i)|$ increases for small n, and reaches a maximum value at a certain time n_c, and then decreases for $n>n_c$. The desynchronization at any site must eventually die away, and synchronization must be recovered for sufficiently large time n. Thus, the synchronization state of Eq. (4) is absolutely stable. In Fig. 2(c) we plot spatiotemporal behaviors of desynchronous elements $\Delta_n(i)=|y_n(i)-x_n(i)|$ ($\varepsilon=0.80$). There are three lines: lines *B* and *D* indicate the lower and upper boundaries of desynchronous region, respectively; line *C* indicates that $\Delta_n(i)$ reach their maximum values at time $n_c(i)$. We are interested in the propagation of desynchronization wave development, i.e., we are interested in the black region of Fig. 2(b). In particular, we will compute the slope of the upper boundary and the height of the right edge of the black area. The latter is nothing but the size of the error avalanche in the output from site N (N can be chosen freely) caused by a single data error at $i=0,n=0$, and this quantity is of great significance for the chaos-based secure communications.

In order to explain the disturbance area of Fig. 2(b), it is important to compute the perturbation propagation and amplification. A quantity of comoving LE can be suitably used for this purpose. In our case the finite time comoving LE can be defined between two sites i and $j>i$, as

$$\mu(i,j,v)=\ln[B^{n_v}A_i]_j/n_v, \tag{5}$$

where B is the Jacobi of coupled map lattice (4), and A_i is a vector of which all the elements are equal to zero except the ith element which takes value equal to 1. The subscript j means to take the jth element from the vector $B^{n_v}A_i$. Moreover, the iteration time n_v is defined on the basis of velocity as

$$v=(j-i)/n_v. \tag{6}$$

The finite time comoving LE of velocity v defines the average exponential rate of perturbation amplification from site i (we will fix $i=0$ afterwards) over space $j-i$ with velocity v [i.e., in time period $n_v=(j-i)/v$]. From Eq. (5), the finite comoving LE depends on i, j, and v. However, due to the symmetry structure of the OCOML system, $\mu(i,j,v)$ depends on $j-i$ and v only in our case, and μ is actually sensitive only to v. In Fig. 3(a), we fix $\varepsilon=0.8$ and plot μ vs v for various $(j-i)$'s. It is remarkable that μ-v curves are insensitive to $(j-i)$'s indeed. From Fig. 3(a), for sufficiently large $j-i$ the finite time comoving LE (5) can be represented, the true (infinite time) comoving LE $\mu(v)=\lim_{j-i\to\infty}\mu(i,j,v)$ in good approximation. In the following we will simply use $\mu(v)$ to denote $\mu(i,j,v)$ in our further discussions. μ varies with v (obviously, $v\leqslant 1$), and μ takes the maximum value μ_M at a certain velocity v_M. By adjusting coupling intensity ε, both μ_M and v_M can be changed. In Fig. 3(b) we plot μ_M against ε. In the two regimes of the figure with minimum μ_M ($0.17<\varepsilon<0.19$ and $0.81<\varepsilon<0.83$), periodic windows are observed. Note that even in stable periodic windows the largest comoving LE is still large than zero. This is possible only for convectively unstable and absolutely stable states.

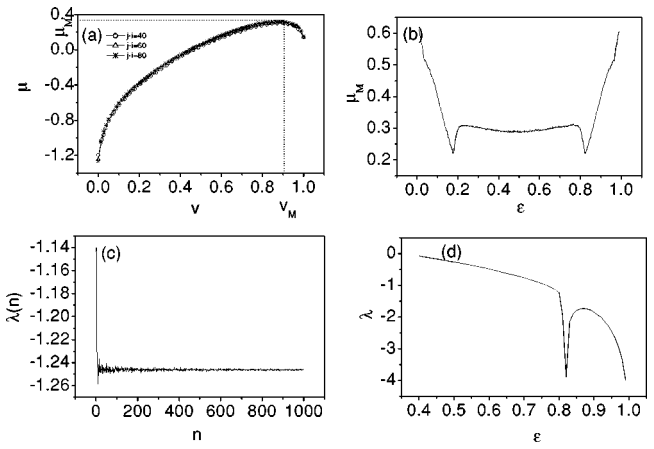

FIG. 3. $\varepsilon=0.8$. (a) Finite time comoving LE $\mu(i,j,v)$ vs velocity v for different $(j-i)$'s. Each plot represents the results of the average of 100 runs. The overlap of curves for different $(j-i)$'s indicates that these finite comoving LEs can well approximate the asymptotic comoving LE $\mu(v)=\lim_{j-i\to\infty}\mu(i,j,v)$. (b) Maximum value μ_M varies with ε. Two minimum parts of the curve ($0.17<\varepsilon<0.19$, $0.81<\varepsilon<0.83$) correspond to periodic windows of the parameter. (c) the finite time largest absolute LE $\lambda(n)$ vs the number of iterations. (d) The largest absolute LE λ vs ε. λ monotonously decreases as ε increases to 1 (apart from the ε regions of periodic windows).

Another quantity relevant to computing perturbation-propagation area is the largest absolute LE λ of the response OCOML system, which can be calculated easily from Eq. (4) as

$$\lambda_i(n)=\ln[B^nA_i]_i/n, \tag{7a}$$

$$\lambda=\lim_{n\to\infty}\lambda_i(n). \tag{7b}$$

Note that while the finite time LE $\lambda_i(n)$ depends on both i and n in Eq. (7a), λ is independent of i in Eq. (7b), i.e., a same λ can be obtained for different i's. In Fig. 3(c) we plot $\lambda_i(n)$ vs n with $\varepsilon=0.8$. $\lambda_i(n)$ approaches a finite negative value quickly as n increases and in Fig. 3(c) $\lambda_i\approx\lambda$ for sufficiently large n. In Fig. 3(d) we plot λ by varying ε. λ monotonously decreases as ε increases to 1 (apart from the ε region of periodic window near $\varepsilon\approx0.82$).

With both well-defined quantities $\mu(v)$ and λ we can now calculate the black area of Fig. 2(b) explicit under certain approximation condition, namely, we can theoretically predict the upper boundary of the black region in Fig. 2(b). Suppose we have a small desynchronous perturbation at $i=0,n=0$,

$$|y_0(i)-x_0(i)|=\delta_0. \tag{8}$$

We assume that the ith site of Eq. (4) is desynchronized from the ith site (1) at time n if

$$|y_n(i)-x_n(i)|\geqslant r,\quad r\leqslant\delta_0 \tag{9}$$

(we will fix $r=\delta_0=10^{-10}$ throughout the paper). Now we try to locate the (i,n) region of desynchronization. Since the perturbation can be amplified most with the largest comoving LE μ_M if the frame moves with velocity v_M, the ith site undergoes the largest desynchronization at time $n=i/v_M$,

$$\delta_{n=i/v_M}(i)\approx\delta_0e^{i\mu_M/v_M}. \tag{10}$$

After time $n=i/v_M$, $\delta_n(i)$ damps with the rate determined by the largest absolute LE λ and the interaction from the site $i-1$. If ε is big (i.e., $1-\varepsilon\ll1$), the interaction from the site $i-1$ shrinks rapidly, we can thus neglect it, and approximately predict the damping of $\delta_n(i)$ as

$$\delta_n(i)\propto\delta_0e^{i\mu_M/v_M}e^{\lambda[n-(i/v_M)]}. \tag{11}$$

The desynchronous region is defined by $\delta_n(i)\approx r$, and this leads to

$$\delta_0e^{(i\mu_M/v_M)}e^{\lambda[n-(i/v_M)]}\approx r,$$

$$n=\frac{i}{v_M}\left(\frac{\lambda-\mu_M}{\lambda}\right)+(\ln r-\ln\delta_0)/\lambda. \tag{12}$$

Since we set $r=\delta_0$, Eq. (12) can be reduced to a simple formula

$$n(i)=\frac{i}{v_M}\left(\frac{\lambda-\mu_M}{\lambda}\right), \tag{13}$$

which specifies the upper boundary of Fig. 2(b). The avalanche size A_N at the site $i=N$ reads

$$A_N=n(i=N)-N=\frac{N}{\lambda v_M}[\lambda(1-v_M)-\mu_M]. \tag{14}$$

It is significant that the desynchronous perturbation propagation behavior and the associated avalanche effect can be explicitly predicted, based on three quantities, the largest comoving LE μ_M, its corresponding velocity v_M, and the largest absolute LE λ.

Generally, the quantities μ_M, v_M, and λ have to be calculated numerically. In case of $1\gg1-\varepsilon>0$, these quantities can be specified explicitly as

$$\mu_M\approx\lambda_0=\lim_{n\to\infty}\frac{1}{n}\sum_{i=1}^{n}\ln|f'(x_i)|=\ln2, \tag{15}$$

with λ_0 being the LE of the single map $x_{n+1}=4x_n(1-x_n)$, and

$$v_M\approx1,\quad \lambda\approx\ln(1-\varepsilon)+\lambda_0. \tag{16}$$

Inserting Eqs. (15) and (16) into Eqs. (13) and (14) we obtain

$$n(i)\approx\frac{i\ln(1-\varepsilon)}{\ln(1-\varepsilon)+\ln2},\quad A_N\approx\frac{-N\ln2}{\ln(1-\varepsilon)+\ln2}. \tag{17}$$

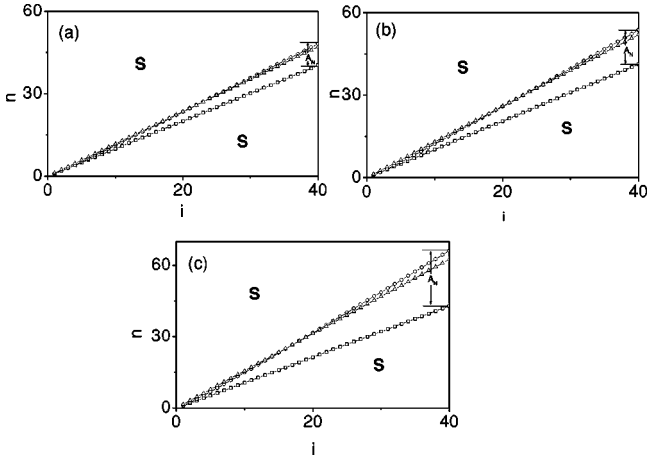

FIG. 4. (a) The same as Figs. 2(b) and 2(c) with $\varepsilon=0.99$. The region between the two S regions denotes the desynchronization area. The squares represent the low boundary of the desynchronous region. The triangles and circles represent the theoretical prediction of the upper boundary of the desynchronization area of Eq. (17) and the corresponding numerical results, respectively. Both results coincide with each other satisfactorily. (b) The same as (a) with $\varepsilon=0.95$. (c) The same as (a) with $\varepsilon=0.90$ with the theoretical results given by Eqs. (13) and (14). Small deviations between the theoretical and numerical results are observed, while qualitative agreement is still identified.

For verifying the validity of Eqs. (13) and (17) we present Fig. 4. In Fig. 4(a) we plot the desynchronous region by taking $\varepsilon=0.99$ and applying the theoretical prediction, Eqs. (17) (triangles) and by direct numerical simulations (circles). Both results coincide practically with each other. In Fig. 4(b), we do the same as Fig. 4(a) with ε reduced to $\varepsilon=0.95$; the theoretical result, Eq. (17), can still predict the perturbation-disturbed desynchronous area satisfactorily. In Fig. 4(c) we do the same as (a) by taking $\varepsilon=0.90$ and applying Eqs. (13) and (14); with this smaller ε, some deviations between the theoretical and numerical results can be clearly seen. However, approximate agreement can be still observed (note, this parameter value is not far from the period window on $0.81>\varepsilon>0.83$). The approximation of Eqs. (13) becomes worse as ε is further reduced due to the reason that Eq. (11), which neglects the interaction from the $(i-1)$th site in computing the quantity $\delta_n(i)$ after $n>i/v_M$, is no longer valid.

In conclusion we have investigated the propagation problem of desynchronous perturbation by considering a one-way coupled lattice model, and obtained analytical results for the desynchronous region and avalanche effect, based on the quantities of the largest comoving LE and the corresponding velocity, and the largest absolute LE. Numerical results well confirm the theoretical analysis in relatively wide parameter region. Though the results have been obtained for a particular one-way coupled map lattice system, the formulas, Eqs. (13) and (14), are expected to be qualitatively valid for general systems of coupled chaotic maps and coupled chaotic oscillators for large couplings with convective instability.

This project was supported by Natural Science Foundation of China under Grants Nos. 10335010 and 10175010, and The Special Funds for Major State Basic Research Projects under Grant No. G2000077304.

[1] L.M. Pecora and T.L. Carroll, Phys. Rev. Lett. **64**, 821 (1990).
[2] E. Ott, C. Grebogi, and J.A. Yorke, Phys. Rev. Lett. **64**, 1196 (1990).
[3] R. Roy, T.W. Murphy, Jr., T.D. Maier, Z. Gills, and E.R. Hunt, Phys. Rev. Lett. **68**, 1259 (1992).
[4] Q.A. Johnson, M. Locher, and E.R. Hunt, Phys. Rev. E **51**, R1625 (1995).
[5] G. Hu and Z.L. Qu, Phys. Rev. Lett. **72**, 68 (1994).
[6] A. Aemengual, E. Hernadez-Garcia, R. Montagne, and M. San Miguel, Phys. Rev. Lett. **78**, 4379 (1997).
[7] L. Kocarev, U. Parlitz, T. Stojnovski, and P. Janjic, Phys. Rev. E **56**, 1238 (1997).
[8] M. Ali and J.Q. Fang, Phys. Rev. E **55**, 5285 (1997).
[9] S. Sinha, Phys. Rev. E **66**, 016209 (2002).
[10] J. Garcia-Ojalvo and R. Roy, Phys. Rev. Lett. **86**, 5204 (2001).
[11] A. Pikovsky, M. Rosenblum, and J. Kurths, *Synchronization: A Universal Concept in Nonlinear Science* (Cambridge University Press, Cambridge, 2001).
[12] S. Boccaletti, J. Kurths, G. Osipov, D.L. Valladares, and C.S. Zhou, Phys. Rep. **366**, 1 (2002).
[13] D. Auerbach, Phys. Rev. Lett. **72**, 1184 (1992).
[14] J.H. Xiao, G. Hu, and Z.L. Qu, Phys. Rev. Lett. **77**, 4162 (1996).
[15] N. Parekh, S. Parthasarathy, and S. Sinha, Phys. Rev. Lett. **81**, 1401 (1998).
[16] Y. Jiang, and P. Parmananda, Phys. Rev. E **57**, 4135 (1998).
[17] K. Kaneko, Phys. Rev. Lett. **65**, 1391 (1990).
[18] F.H. Willeboordse and K. Kaneko, Physica D **86**, 428 (1995).
[19] K. Konishi, H. Kokame, and K. Hirata, Phys. Lett. A **263**, 307 (1999).
[20] I.S. Aranson, L. Aranson, L. Kramer, and A. Weber, Phys. Rev. A **46**, R2995 (1992).
[21] I. Aranson, H. Levine, and L. Tsimring, Phys. Rev. Lett. **72**, 2561 (1994).
[22] G. Hu, J.H. Xiao, and J.H. Gao, Phys. Rev. E **62**, R3043 (2000).
[23] S.H. Wang, J.Y. Kuang, J.H. Li, Y.L. Luo, H.P. Lu, and G. Hu, Phys. Rev. E **66**, 065202 (2002).
[24] S.H. Wang, W.P. Ye, H.P. Lu, J.Y. Kuang, J.H. Li, Y.L. Luo, and G. Hu, Commun. Theor. Phys. **40**, 57 (2003).